FEBS Letters 579 (2005) 2026–2034 FEBS 29400

Hypothesis

Simulating redox coupled proton transfer in cytochrome *c* oxidase: Looking for the proton bottleneck

Mats H.M. Olsson*, Pankaz K. Sharma, Arieh Warshel*

Department of Chemistry, University of Southern California, 3620 McClintock Avenue, Los Angeles, CA 90089-1062, USA

Received 23 December 2004; revised 12 February 2005; accepted 14 February 2005

Available online 11 March 2005

Edited by Maurice Montal

Abstract **Gaining a detailed understanding of the molecular nature of the redox coupled proton transfer in cytochrome *c* oxidase (COX) is one of the challenges of modern biophysics. The present work addresses this by integrating approaches for simulations of proton transport (PTR) and electron transfer (ET). The resulting method converts the electrostatic energies of different charge configurations and reorganization energies to free-energy profiles for different PTR and ET pathways. This approach provides for the first time a tool to study the actual activation barriers and kinetics of different feasible PTR processes in the cycle of COX. Using this tool, we explore the PTR through the bottleneck water molecules. It is found that a stepwise PTR along this commonly assumed path leads to far too high barriers and is, thus, inconsistent with the observed kinetics. Furthermore, the simulated free-energy profile does not provide a simple gating mechanism. Fortunately, we obtain reasonable kinetics when we consider a PTR that involves a concerted transfer of protons to and from E286. Finally, semi-qualitative considerations of the forward and backward barriers point toward open questions about the actual gating process and offer a feasible pumping mechanism. Although further studies are clearly needed, we believe that our approach offers a general and effective tool for correlating the structure of COX with its function.**

© 2005 Federation of European Biochemical Societies. Published by Elsevier B.V. All rights reserved.

Keywords: Cytochrome *c* oxidase; Proton pumping; EVB; Coupled ET/PT

1. Introduction

Coupled electron transfer/proton transfer (ET/PT) plays a central role in energy conversion in living systems and is considered as key elements in bioenergetics. A prominent example is provided by cytochrome *c* oxidase (COX). This protein couples the four electron reduction of O_2 to water and *trans*-membrane PT, e.g. [1–3], which results in an electrochemical proton gradient that drives ATP synthesis. The structure of COX [4,5] and many other studies (for recent reviews see [6,7]) provide the opportunity to describe biological ET/PT on a molecular level.

In trying to obtain a detailed structure–function correlation for COX it is important to understand the energetics and the time dependence of the pumping process. This challenge can be addressed by computer modeling approaches and some elements of the COX reaction have already been examined by simulation methods [8–10]. However, the relationship between the protein structure, the PTR energetics and directionality has not been established. For example, the calculations of Olkhova et al. [9] provided important insight about the electrostatic coupling but did not address the energetics of the pumping process. The chemical steps were recently studied by detailed quantum mechanical calculations [11], but this instructive study did not explore the energetics of pumping the protons across the membrane. The insightful study of Wikstrom et al. [8] attempted to establish a gating mechanism by considering the orientation of the water molecules in the hydrophobic region between heme a and heme a3, but this study did not explore the actual PTR process. Nevertheless, this work raised a crucial question about the nature of the gate that controls the uphill PTR. The nature of the pumping process was eloquently considered by Mills and Ferguson-Miller [12] who assessed the evidences for direct and indirect coupling mechanism, where the indirect mechanism involves conformational and pK_a changes. The details of a conformational mechanism have been considered by Brzezinski and coworkers [7,13]. Although this proposal has appealing aspects, it cannot be verified without specific tools of converting structures to pK_a values.

In order to elucidate the molecular nature of the PTR in COX it is essential to have a theoretical framework that relates the actual structure of this system to its pumping action. Such a general formulation has been developed in out early studies of PTR [14–16] and ET [17,18] and is used here to study the coupled ET/PT process in COX. In doing so we focus on illustrating key concepts and on examining the nature of the PTR process and the role of E286, which is assumed to be a key junction along the PTR paths. It is found that the commonly assumed transient deprotonation of E286 leads to far too high barriers when it occurs in a stepwise mechanism. However, a concerted path appears to provide reasonable barriers without requiring E286 to be deprotonated. This path appears also to help in exploring the nature of a plausible gating mechanism.

*Corresponding authors. Fax: +1 213 740 2701.
E-mail address: molsson@usc.edu (M.H.M. Olsson).

Abbreviations: COX, cytochrome *c* oxidase; PTR, proton transport; EVB, empirical valence bond; LRA, linear response approximation; PDLD/S, protein dipole Langevin dipole/semi-macroscopic

0014-5793/$30.00 © 2005 Federation of European Biochemical Societies. Published by Elsevier B.V. All rights reserved.
doi:10.1016/j.febslet.2005.02.051

2. Concepts and methods

In order to describe our methods and concepts it is useful to start by reviewing several basic features of the system studied. Thus, we start by a schematic description of COX (Fig. 1) and by focusing on the transfer of H^+ from E286 to Prd (a3) and the iron-bound oxygen (see right panel Fig. 1).

Since we are mainly concerned with conceptual aspects here we will only examine parts of the overall cycle of COX. These parts will, however, contain all the elements of the coupled ET/PT. More specifically, we will study a series of reactions that can be described schematically in Fig. 2 following a recent study of Siegbahn et al. [11]. The description in Fig. 2 is rather schematic and some of the details might still be uncertain. For example, some workers, e.g. [13], favors PTR to the iron-bound oxygen before the PTR to Prd. Nevertheless, Fig. 2 still provides a framework for addressing the key problems. Note, however, that the sequence of events between each step in Fig. 2 (e.g., the PTR and ET pathways) is not established and must be explored by more detailed considerations. In order to do so effectively, we introduce here a short hand notation (Fig. 3) that relates the structure of the system to the specific occupation of the ET chain and the PTR chain.

A coupled ET/PT processes can be described by using Marcus' type state diagrams in the quantitative framework of the empirical valence bond (EVB) approach [19]. In this description, we start by combining our early picture of ET [17] and PT [14,15] and obtain a general expression for the free energy of each feasible state of the system by

$$\Delta G^{(m)} = \sum_i \left\{ -2.3RTq_i^{(m)}\left[\mathrm{p}K^{\mathrm{p}}_{\mathrm{int},i} - \mathrm{pH}\right] + \sum_k \mid q_k^{(m)} \mid \Delta I^{\mathrm{w}}_{k,q^{(m)}} + \frac{1}{2}\sum_{i\neq j} w_{ij}q_i^{(m)}q_j^{(m)} \right\}, \quad (1)$$

where m designates the vector of the charged states of the given configuration, i.e., $m = (q_1^{(m)}, q_2^{(m)} \ldots q_n^{(m)})$. "$i$" runs over the site of proton donors and acceptors, "k" over the sites of electron donor and acceptors and "j" runs over both the "i" and "k" series. Here, $q_i^{(m)}$ is the actual charge of the ith group at the mth configuration. This can be 0 or −1 for acids and 0 or 1 for bases (where we for simplicity restrict our formulation to mono ions). $\Delta I^{\mathrm{w}}_{k,q}$ is the free energy of forming the charged form of the kth group from its uncharged group in solution (this free energy is obtained from the corresponding reduction potential). The $W_{ij}q_iq_j$ term represents the charge–charge interaction effect. The intrinsic pK_{a} (pK_{int}) is the pK_{a} that the given ionizable group would have if all other ionizable groups were kept at their neutral state (the evaluation of this term is described in [20]). Eq. (1) can also be expressed in terms of the energy of forming the given configuration in a reference state (in this case in aqueous solution) at infinite separation of the ions and then transforming it into the protein. This gives, see, e.g. [14,17],

$$\Delta G^{(m)} = \sum_i \left\{ -2.3RTq_i^{(m)}\left[\mathrm{p}K^{\mathrm{w}}_{\mathrm{a}} - \mathrm{pH}\right] + \mid q_i^{(m)} \mid \left(\Delta\Delta G^{\mathrm{w}\to\mathrm{p}}_{\mathrm{solv}}\left(q_i^{(m)}\right)\right)_0 \right\} + \sum_k \left\{ \mid q_k^{(m)} \mid \Delta I^{\mathrm{w}}_{k,q^{(m)}} + \mid q_k^{(m)} \mid \Delta\Delta G^{\mathrm{w}\to\mathrm{p}}_{\mathrm{solv},0}\left(q_k^{(m)}\right) \right\} + \frac{1}{2}\sum_{j\neq j'} \Delta G_{jj'}, \quad (2)$$

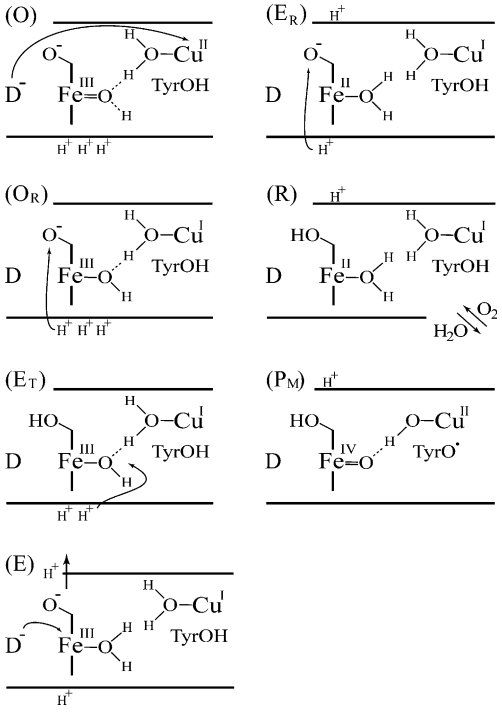

Fig. 2. The steps examined in the present study. The specific steps are based on the study of Siegbahn et al. [11].

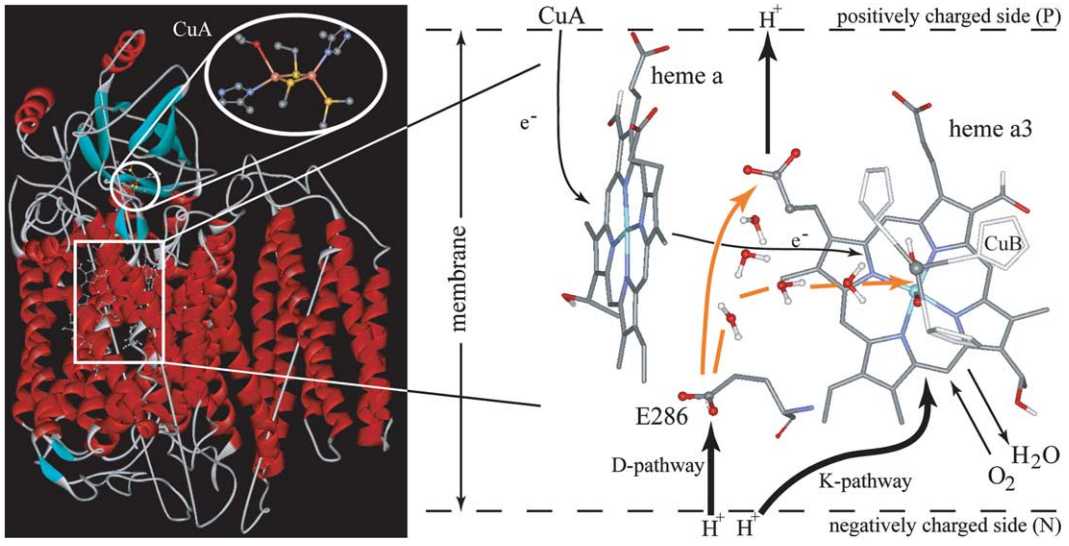

Fig. 1. A schematic description of the key elements in the COX systems. The figure considers heme a, heme a3, the two sides of the membrane, the entry and the exit proton pathways. The pathways explored here are shown in orange in the right side of the diagram.

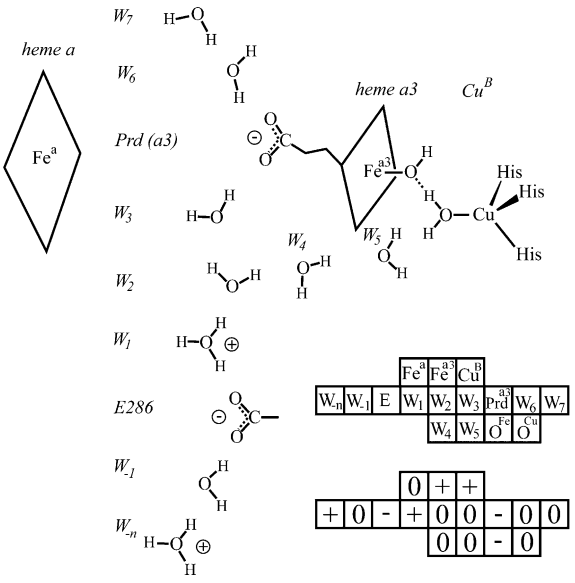

Fig. 3. Illustrating the notation used in our state diagrams. The figure depicts the groups included in the present study and the label used for each group. The joint boxes in the lower part illustrate our shorthand notation where we arrange our diagram according to the order of each element and designate each state by its charged state. The upper row depicts the electron population on the redox centers (heme a, heme a3 and CuB centers), the middle row shows the protonation state of the vectorial pK_a groups from the N-side to the P-side, and the lower row shows the protonation state of the pK_a groups to the bound oxygen.

where $(\Delta\Delta G^{w\to p}_{solv}(q_i))_0$ represents formally the energy of moving q_i from water to its actual protein site when all other ionizable groups are neutral. The solvation of the uncharged form of a given group is also included in $\Delta\Delta G_{solv}$ in the actual calculation [20].

The activation free energy for a transfer from state m to state m' can now be evaluated by the EVB concepts and Eq. (2). This allows us to describe any system and its dependence on the general solvent coordinate. This is illustrated in Fig. 4 for a simple hypothetical coupled ET/PT process. In this case an ET reaction between two quinone molecules is coupled to a PT between an acidic group and an amine. The two upper boxes designate the electron population of the redox active groups, whereas the two lower boxes depict the protonation state of the pK_a active groups. The ET/PT reaction can be followed by the arrows indicating the individual transfer steps. In this example, the initial step is an ET between the two quinone molecules from state (I) to state (II). In a second step the proton is transferred from the carboxylic acid to the amine giving rise to state (III). The diabatic and adiabatic surfaces are shown in solid and dashed lines, respectively. The same approach can be used for any general case as is illustrated in Fig. 5, where we consider a proton being transferred from E286 to Prd a3 in COX (reaction $O \to E_R$) via intermediate states where the proton resides on intervening water molecules. The first step is also accompanied by an ET between two redox centers. Again, the protonation state of the system can be seen from the connected boxes and electron and PTs can be followed by the small arrows (a more compact notation is used in the upper configuration state where the consecutive PTR is indicated with an arrow).

In principle, we can evaluate the free-energy functions for each transfer by the EVB microscopic simulations and run time-dependent simulations by using a simplified EVB/LD model [21]. Here, however, we are mainly interested in the energetics and can thus use a semi-quantitative estimate for each step. For example, when the transfer from m to m' involves only one PT or one ET, the activation energy is given by [21]

$$\Delta g^{\ddagger}_{m,m'} = \frac{(\Delta G_{mm'} + \lambda_{mm'})^2}{4\lambda_{mm'}} - H_{mm'} + \frac{H^2_{mm'}}{(\Delta G_{mm'} + \lambda_{mm'})}, \tag{3}$$

where $\Delta G_{mm'}$ is the free-energy change for transfer between state m and m', and $\lambda_{mm'}$ is the corresponding reorganization energy (that can be evaluated as described elsewhere [19]). $H_{mm'}$ is the off-diagonal element that mixes the states m and m'. This term is taken as the EVB coupling term for PT between a donor and acceptor and the relevant coupling term (the tunneling matrix element) for an ET step. The proper coupling can also be evaluated for a concerted PT and for an ET/PT process.

The rate constant for each step is obtained by using transition state theory (see, e.g. [19]) for adiabatic PT steps and the semi-classical treatment of diabatic ET theory (see, e.g. [22]) for the ET steps. That is, we use

$$k^{PT}_{mm'} = \frac{k_B T}{h} \exp\left\{-\frac{\Delta g^{\ddagger}_{mm'}}{k_B T}\right\}, \tag{4a}$$

$$k^{ET}_{mm'} = \left(\frac{H_{mm'}}{\hbar}\right)^2 \left(\frac{\pi\hbar}{k_B T \lambda}\right)^{\frac{1}{2}} \exp\left\{-\frac{\Delta g^{\ddagger}_{mm'}}{k_B T}\right\}, \tag{4b}$$

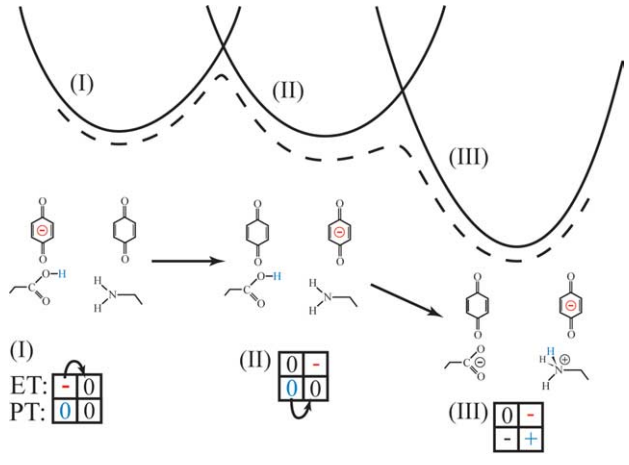

Fig. 4. Showing a simple example of our compact notation for a coupled electron and proton transfer. The electron and proton populations are, respectively, given by the upper and lower rows of boxes. In this example, an ET between the two quinones, (I) → (II), and the subsequent PT, (II) → (III), can be followed by the curved arrows and color coding (red for ET and blue for PT).

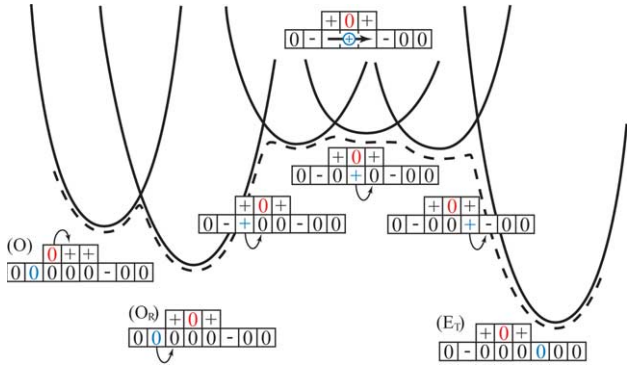

Fig. 5. Showing a schematic description of the $O \to E_T$ step in COX via intermediate states where the proton resides on intervening water molecules. As previously, the electron and proton transfers are given by the upper and lower rows of boxes, respectively. For convenience we have grouped the charge on the water molecules before E286 in the first second-row box. In the upper part of the figure, we have condensed several subsequent transfers between water molecules by representing it with an arrow with a '+' sign in a single state diagram. Again, the diabatic and adiabatic surfaces are shown in solid and dashed lines, respectively.

where $\Delta g^{\ddagger}_{mm'}$ for PT steps can include nuclear quantum mechanical (NQM) corrections (e.g., zero point energy and tunneling) [23]. Similarly when needed we can evaluate NQM corrections for $\Delta g^{\ddagger}_{mm'}$ for ET steps [24]. In case of a coupled ET/PT process we should determine if we have an adiabatic or a diabatic process and choose the preexponential term accordingly [22]. In the present case, however, we will use a simplified treatment (see below).

With the above picture in mind we can focus on the $\Delta G_{mm'}$, which determine the trend in the corresponding $\Delta g^{\ddagger}_{mm'}$ term. The evaluation of this term depends, as is clear from Eq. (2), on the relevant reduction potentials and pK_a values as well as on the $\Delta\Delta G_{solv}$ and the $W_{jj'}$ terms. The most crucial term is the $\Delta\Delta G_{solv}$ solvation term. This term is evaluated by the linear response approximation (LRA) version of the semi-macroscopic protein dipoles Langevin dipole model (PDLD/S). Since this approach, the PDLD/S-LRA, has been used in studies of pK_a values and reduction potentials in proteins and discussed extensively elsewhere, e.g. [20,25,26], it will not be addressed here. The $W_{jj'}$ interaction term is evaluated using

$$\Delta G_{jj'} = \frac{332 \cdot q_j \cdot q_{j'}}{\varepsilon^{jj'}_{\text{eff}}(r_{jj'}) \cdot r_{jj'}}, \tag{5}$$

where $\Delta G_{jj'}$ is given in kcal/mol, $r_{jj'}$ is the distance (in Å) between groups j and j' and $\varepsilon_{jj'}(r_{jj'})$ is an effective dielectric function for the charge–charge interaction given by

$$\varepsilon^{jj'}_{\text{eff}} = 1 + \varepsilon'(1 - \exp\{-\mu r_{jj'}\}), \tag{6}$$

where we use ε' and μ values of 40 and 0.18 (we have also used other values of ε' to establish the upper and lower limits of our conclusions). The physical justification of Eq. (6) and the reliability of our $\varepsilon_{jj'}$ have been discussed in previous studies, e.g. [20].

The pK_a values and reduction potentials of the ionizable groups in Eq. (2) were obtained (see Table 1) with the PDLD/S-LRA approach according to standard protocol using the MOLARIS program [27] (see also [28] and references therein). Starting from the X-ray structure of COX (pdb entry 1M56 in the Brookhaven protein database [29]), the pK_a values and reduction potentials were averaged over 50 protein configurations that were obtained at each 1 ps from a 50 ps molecular dynamics simulation. The simulations used the ENZYMIX force-field and a step-size of 0.5 ps. The effect of the low dielectric of the membrane was not considered since the distance to the membrane region from most of the groups studied is relatively large (a more consistent study will be used in the future).

In exploring the effect of the redox centers we held the metal centers with strong constraints and spread the charges of the heme on the iron and the attached nitrogen atoms (rather than over the whole heme system). The validity of this approximation has been established in earlier studies of redox systems, e.g. [30]. The changes in $\Delta I^{w} + \Delta\Delta G_{solv}$ for ET from heme a to heme a3 was found to be ~ -5 kcal/mol by PDLD/S-LRA calculations. The corresponding value for ET from heme a to the Cu system was chosen rather arbitrarily as -5 kcal/mol to provide a downhill gradient. In principle we could have evaluated this value more systematically as was done before [28]. We could also obtain the relevant value from experimental studies (e.g. [31]).

Table 1
Interaction energies between elements of our active space[a]

ε'=40	E286	W1	W2	W3	W4	W5	Prd	OH	Fe(a)	Fe(a3)	Cu_B
E286	13.9	-7.5	-3.3	-1.7	-2.8	-1.6	1.0	1.0	-0.6	-0.9	-1.1
W1	-7.5	-10.2	9.7	3.0	4.5	1.8	-1.3	-1.0	0.7	0.9	1.2
W2	-3.3	9.7	-10.2	8.6	13.8	2.7	-2.0	-1.2	0.7	1.1	1.3
W3	-1.7	3.0	8.6	-13.1	5.8	2.3	-4.4	-1.2	0.9	1.1	1.3
W4	-2.8	4.5	13.8	5.8	-10.2	6.0	-2.2	-1.8	0.7	1.5	2.2
W5	-1.6	1.8	2.7	2.3	6.0	-8.1	-1.8	-4.4	0.6	3.1	6.5
Prd	1.0	-1.3	-2.0	-4.4	-2.2	-1.8	5.1	1.3	-0.9	-1.3	-1.3
OH	1.0	-1.0	-1.2	-1.2	-1.8	-4.4	1.3	2.8	-0.6	-31.5	-4.5
Fe(a)	-0.6	0.7	0.7	0.9	0.7	0.6	-0.9	-0.6	0.0	0.7	0.5
Fe(a3)	-0.9	0.9	1.1	1.1	1.5	3.1	-1.3	-31.5	0.7	-5.0	2.8
Cu_B	-1.1	1.2	1.3	1.3	2.2	6.5	-1.3	-4.5	0.5	2.8	-5.0

[a]The table gives the interaction energies, the intrinsic pK_a values[b] (expressed in terms of the free energies of moving a proton from the given site to a reference bulk solution at pH = 0.0) and the intrinsic reduction potentials[b] for the components of our active space. The interaction energies are given for $\varepsilon' = 40$ for the case when the interacting groups are at their charged state. The results for $\varepsilon' = 20$ can be estimated by multiplying the corresponding values by a factor of two. Both the "intrinsic" pK_a values and the reduction potentials reflect the effect of groups out of the active region (so they are apparent values with regard to the groups outside the active region). The pK_a value for the Fe bound to OH is taken from [11]. The free energy of moving the electron from Fe (a) to Fe (a3) was estimated by PDLD/S calculations to be -5 kcal/mol. In these calculations we arbitrarily chose the free energy of moving the electron from Fe (a) to the Cu atom to be the same (-5 kcal/mol). This was done since the specific selection did not change our results with regards to the free energy of the PTR process (see text). The interaction energies (the $\Delta G_{jj'}$ of equation (2)) is given as off-diagonal terms in the table.

[b]Note that the diagonal elements are also given in kcal/mol. The pK_a values are 10.1, −7.4, −7.4, −9.5, −7.4, −5.9, 3.7, 2.0 in pK_a units, respectively, for E286, W1, W2, W3, W4, W5, Prd and OH, while the reduction potentials are 0, 200 and 200 mV (see text). The chemical energy associated with the $R \rightarrow P_M$ step is taken as -4 kcal/mol.

However, since the free-energy profiles for the PTR steps were not sensitive to the redox gradient we left the evaluation of the redox energies to subsequent studies. The energy of the $R \rightarrow P_M$ "chemical" step was taken as −4 kcal/mol from [11]. The $H_{mm'}$ and the $\lambda_{mm'}$ for the PT steps were taken initially from our previous studies [14–16] but in most cases we found that the resulting barrier does not change the profile obtained by considering the corresponding free energy difference (the $\Delta G_{mm'}$) by more than 1 kcal/mol. We will thus present our results using $\Delta G_{mm'}$ as equivalent to $\Delta g^{\ddagger}_{mm'}$.

3. Results

In order to evaluate the energy of the relevant states, we need to start by calculating the pK_a values and reduction potentials of the relevant ionizable groups. Table 1 provides the apparent pK_a values and apparent reduction potentials (note that the unit is kcal/mol rather than pK_a units and mV) as well as the coupling between the groups included in the active space. We also considered the limit of $\varepsilon' = 20$, which we consider as the upper limit for the change in charge interaction (the reader may estimate the results for $\varepsilon' = 20$ by multiplying the corresponding values from Table 1 by a factor of two). The apparent pK_a values do not include the interaction between the molecules on the active region, but is included in the final state energy diagrams. As seen in the table, there is significant coupling between the different sites although it is smaller than that obtained by the discretized continuum calculations of Kannt et al. [32] (as explained in [20] the use of low dielectric constant in such studies may lead to an overestimate of ΔG_{ij}). However, the main issue is the conversion of the information in Table 1 to free-energy diagrams and the use of this information in the examination of the pumping process of COX. This will be considered next.

We start our analysis by considering a stepwise PTR for the $O_R \rightarrow P_M$ step and the corresponding results are described in Fig. 6. In the diagram, we focus on the energy of the different states rather than on the barrier between different states since the $\Delta g^{\ddagger}_{mm'}$ are similar to the corresponding $\Delta G_{mm'}$. We also note that our diagram assumes the presence of two protons in the D-pathway where one of them is located on W_{-1} (this simplified assumption will be shown to underestimate the overall barrier). At any rate, the path depicted in Fig. 6 seems to describe a "proper" downhill process. Unfortunately, however, this diagram involves several problems. First, the forward barrier for PTR from E286 to Prd (a3) is far too high to be consistent with the kinetics of COX. That is, the activation barrier for the $O_R \rightarrow E_T$ step is more than 22 kcal/mol, which corresponds to a rate constant of less than 10^{-3} s^{-1} (using transition state theory) while the overall kinetics of COX is in the range of 10^3 s^{-1}. This problem (which will eventually become more severe once we consider the transfer from W_{-n}) reflects the fact that E286 has a high pK_a value (the experimental estimate is 9.4 [7]) and that it has to transfer a proton to water molecules in a hydrophobic environment. Second, the diagram in Fig. 6 does not consider the process of moving the proton back from the bulk water on the positive side to Prd a3, back to E286, and finally to the negative side. This back reaction may occur at different steps of the reaction and prevent the overall PTR from the N to the P side. To illustrate this problem, we consider in Fig. 7 the PTR from W_7 to W_{-n} for state E'_R. We also consider schematically a transfer from P to W_{-n}, assuming that the barrier from P to W_7 is not very high since it involves a PTR in polar environment (this assumption should, however, be examined by actual calculations). The figure demonstrates that the proton is not blocked from going backward by either the reaction barriers or the overall energetics. This problem remains despite the electrostatic effect of the charge change of

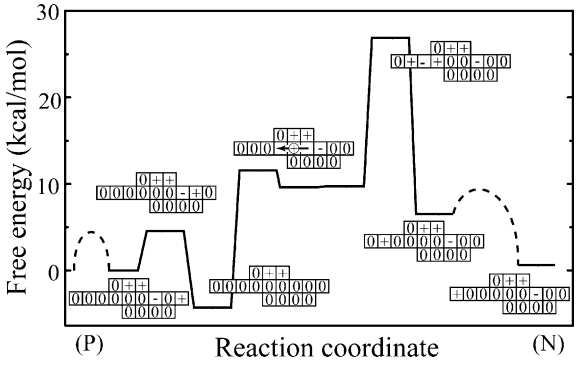

Fig. 7. The energetics of a stepwise PTR from W_7 to W_{-n} in E'_R. The figure demonstrates that the energetics for a proton on the P and N side is similar so that the proton can move forward and backward. Of course we have a barrier which is inconsistent with the observed kinetics. The profile for the PT from W_0 to W_{-n} and from W_7 to the P side are hypothetical since the work did not examine the energetics along the D pathway or the barrier along the exit channel.

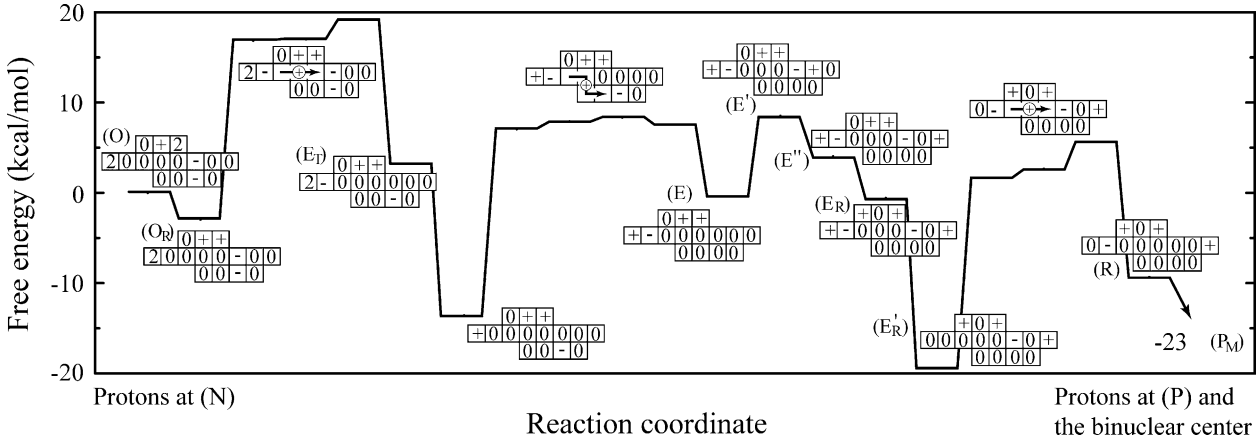

Fig. 6. The energetics obtained with a stepwise PTR for the $O \rightarrow P_M$ process.

the redox centers and the pK_a value of Prd a3 since the electrostatic effects are not significant when we approach the bulk on the P side. The same problem also remains in state P_M. With this is mind, we may conclude that the system does not provide a "gate" and cannot sustain uphill proton pumping. That is, despite the fact that the free energy of moving from state O to P_M or from O to E is downhill, we find that in state E'_R the proton can move from P to N with similar probability as moving from P to N. Of course, as was also stated above, the barrier is too high to be consistent with the observed kinetics, but with a given barrier we do not have a way to create a different energetics for the initial and final state.

The considerations of the stepwise PTR in Figs. 6 and 7 raise a major challenge to the idea that E286 provides a crucial junction for the PTR process and the vectorial PTR. Fortunately, we obtain a very different picture when we consider the concerted process. To see this point we first consider the problem of having too high barrier in the $O_R \rightarrow E_T$ step. As is shown in Fig. 8, when we consider this step while allowing the concerted proton motion E286 $\rightarrow W_0$ and $W_{-1} \rightarrow$ E286, we obtain a $\Delta G^0 \approx 5$ kcal/mol and $\Delta g^{\ddagger} \approx 7$ kcal/mol (estimated by a 3×3 EVB Hamiltonian), giving a rate constant of about $5 \times 10^7\ s^{-1}$. Obviously, we are required to consider a transfer from W_{-n} in order to determine the larger overall forward barrier, which will be done below.

As indicated by the discussion of the stepwise profile it is important to consider the overall PTR profile for the $W_{-n} \rightarrow W_7 \rightarrow$ P path. This is done in Fig. 9 for the E'_R state, where we obtain an overall reasonable barrier (about 13 ± 3 kcal/mol) with a rate constant of about $10^4\ s^{-1}$. As stated above, this estimate is based on the assumption that the barrier for PTR from P to W_7 is not very high.

In principle, we should be able to use the profiles of the type depicted in Figs. 8 or 9 in simplified EVB Langevin dynamics simulations [21] or a master equation [15] and to calculate the H^+ current. However, this type of study is out of the scope of the present paper where we consider the gating in a very qualitative way. Thus, we only try to approximate the forward and backward kinetics by a Michaelis–Menten type of kinetics, writing

$$v_+^{(N\rightarrow P)} \approx \frac{k_{VI\rightarrow IV} \cdot [H^+]_N \cdot [E]}{K_{VI\rightarrow B(N)} + [H^+]_N}, \tag{7a}$$

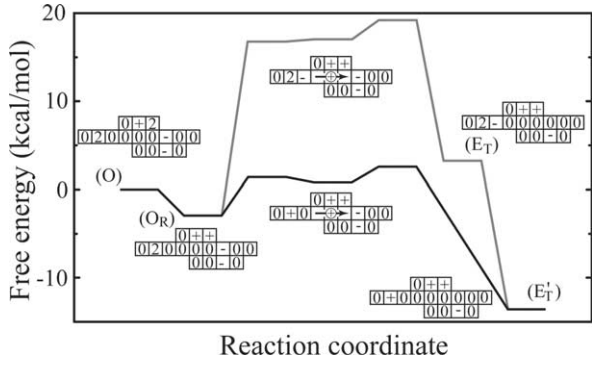

Fig. 8. The energetics of a concerted path in the $O_R \rightarrow E_T$ step. In this case we have only a small barrier for the forward process. The profile for the stepwise process is given by a gray line.

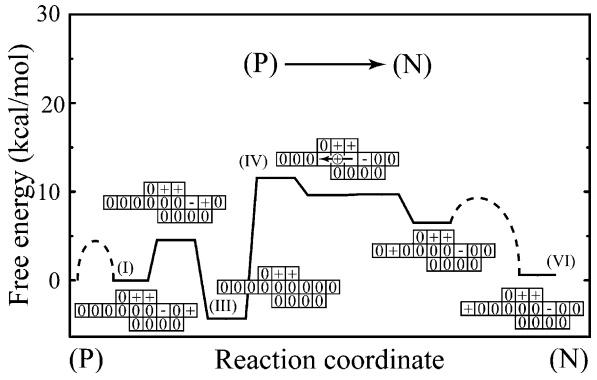

Fig. 9. The energetics of a concerted PTR from W_7 to W_{-n} in E'_R.

$$v_-^{(P\rightarrow N)} \approx \frac{k_{III\rightarrow IV} \cdot [H^+]_P \cdot [E]}{K_{III\rightarrow B(P)} + [H^+]_P}, \tag{7b}$$

where $k_{III\rightarrow B(P)}$ is the equilibrium constant of moving the proton from W_{-n} to the bulk. If we have a trap at state III, as the present calculations indicate, $[H^+]_P$ can be larger than $K_{III\rightarrow B(P)}$ while $[H^+]_N$ can still be smaller than $K_{IV\rightarrow B(N)}$. This will give

$$v_+ \approx \left(\frac{k_{VI\rightarrow IV}}{K_{VI\rightarrow B(N)}}\right) \cdot [H^+]_N \cdot [E], \tag{8a}$$

$$v_- \approx k_{III\rightarrow IV} \cdot [E]_P, \tag{8b}$$

leading in some cases to the situation where $v_- < v_+$. This can provide a gating mechanism since the effective barrier from III to IV is larger than that from VI to IV. Of course, a more careful analysis is required to establish this possibility including a detailed evaluation of the proton profile in path D and eventually full master equation or Langevin dynamics kinetic treatment.

4. Concluding remarks

In this work, we have explored key aspects of the nature of the PTR process in COX by using a microscopically based model with a special emphasis on the energetics of the PTR process. Our model determines the reduction potentials and the pK_a values of the key elements of the system and uses them to evaluate the free energies of the relevant states. The relevant activation barriers were then estimated using a modified Marcus' treatment. Our study led to several significant results. First, it was found that the energetics of a stepwise ET/PT leads to barriers that are inconsistent with the observed kinetics. Second, it is found that a simple concerted PT (where the energy spent in pushing a proton from a trap on an acid to a water molecule is returned in part by a PT from another water molecule to the same acid) leads to a reasonable kinetics. Finally, considering forward and backward barriers of the concerted path, we envision tentative conditions for a gating mechanism (further considerations will be given below). Establishing these possibilities, however, requires a more detailed kinetic analysis and it is possible that the actual gating mechanism still presents an open question. The main point, however, is that our approach allows us to examine the validity

of different proposals for the gating mechanism and equally important provides a general tool for examining the nature of the redox coupled PTR in COX.

It is useful to note that our general strategy, which was introduced quite early [14,15] is based on examining the energetics of a large number of charge states. A conceptually similar strategy was used successfully in exploring permeation mechanism [33] and in exploring the ion current in this channel [34]. More directly related studies that consider simulations of PTR in proteins have also been reported [21].

The origin of the gating mechanism in COX has been the subject of significant recent interest [7,8,12,13] but none of the recent studies have evaluated the actual barriers for the PTR process. For example, Wikstrom et al. [8], who considered the orientation of the water molecules in the hydrophobic region between heme a and heme a3, have raised the important issue of the gating mechanism. However, the actual energetics of the PTR process was not examined. The nature of the gating mechanism was also discussed by Namslauer and Brzezinski [13], who proposed a mechanism that couples conformational changes and pK_a changes. This mechanism considered a transient reduction in the pK_a value of E286 coupled with an increase in the pK_a value of a group on the P side and conformational changes that lead to a change in the hydrogen bonding connectivity and helps in providing a gating process. Apparently, as found in this work, there is no need for a transient reduction of the pK_a value of E286 because of the effectiveness of the concerted PTR.

The present work identified a concerted PTR as the mechanism that allows the system to transfer protons through Glu 286. Since some readers might associate this finding with the issue of the importance of the so-called Grotthuss mechanism in biological PTR, we would like to reclarify our view. The Grotthus mechanism requires a proper orientation of the water molecules, and such orientations are *indeed* involved in the actual PTR obtained by EVB simulations. However, our point is that the energy of orienting the non-polar water molecules to a proper arrangement is trivial compared to the changes of the electrostatic energy of the proton in different sites (the $\Delta G_{mm'}$ of Eq. (3)). Thus PTR in proteins are determined by the electrostatic energy and not by the free energy of reorienting the unionized water molecules (see [14–16]). Now, as explained in [21], when we have three sites, where the proton energy is high in the central site and low in the first and last sites, we find indeed that a concerted PTR allows the system to overcome the electrostatic barrier in the central site. However, once the stepwise barrier involves two or more high energy sites the concerted transfer cannot help to overcome this barrier. At any rate, the electrostatic energy that determines the energy of the different states (rather than the orientation of the non-protonated water molecules) is the key factor in the control of PTR processes in proteins.

A very recent work [37] has used some of the concepts introduced in our early works (Eq. (2)) but did not explore the energetics of the proton on the internal water molecules. This work suggested that the changes in the pK_a of the Cu-bound His 291 (due to protonation of the Fe-bound OH) can control the pumping process. However, examining this instructive suggestion identified several potential problems. First, it is not entirely clear that a His bound to a positively charged Cu^+ or Cu^{2+} has a sufficiently high pK_a to be a part of a PTR chain. Second, and perhaps more importantly, adding His 291 to our diagrams did not eliminate the problems pointed out by the analysis in Figs. 8 and 9. That is, increasing the proton energy on His 291 does not change the energy of the proton on the N and P sides, in the same way that the stabilization of the ionized Prd by a migration of proton to the Fe-bound OH does not provide a gate. In particular, it is hard to see how this can be accomplished with His 291, since a concerted back transfer ($W_8 \rightarrow$ His, His $\rightarrow$ Prd and then a transfer through W_3, where W_8 is a water molecule

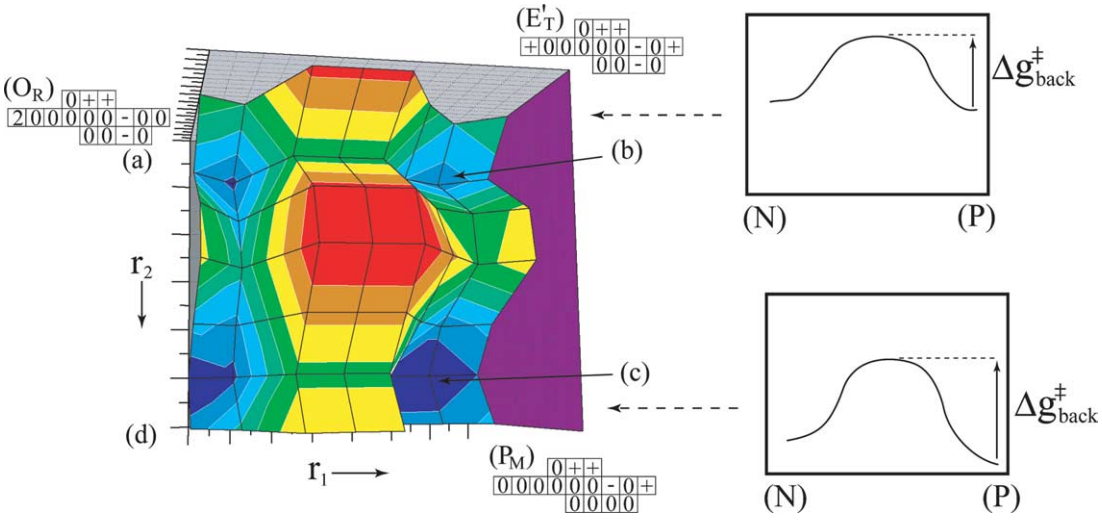

Fig. 10. A tentative mechanism that may rationalize the gating process. The figure presents a two-dimensional free-energy diagram where r_1 and r_2 correspond, respectively, to the transfer of the first and the second proton. The blue and red represent low and high free-energy regions, respectively. Changing r_1 while keeping the r_2 fixed moves the proton from its initial position at N to W_7 or to P. Changing r_2 from point b to point c leads to protonation of the iron-bound OH and to state P_M. Now, if the interaction between the binuclear center and the hydrophobic water chain is sufficiently large, the barrier for moving from c to d will be larger than the barrier for moving from b to a (and from a to b) and we will have a vectorial process driven in part by the downhill chemical step.

near His291) will lead to a similar barrier to the corresponding forward reaction.

Despite the above arguments it is clear that we have not explored the possibility [7,13] that conformational changes contribute to the gating mechanism. Now, although this mechanism, by itself, cannot be established (or eliminated) without evaluating the structures of different conformational states, the present study indicates that such changes might not explain the pumping process. That is, the electrostatic consequences of structural changes can be examined in an indirect way since such effects follow the corresponding changes in charge–charge interactions, e.g. [35]. For example, when a positive charge of an ion pair is neutralized, the dipoles near the negative charge rearrange to compensate for the missing effect of the missing positive charge. This type of conformational change appears to be very general. Thus, the effect of electrostatic induced conformational changes can be estimated by scaling the given change in charge–charge interactions with different effective dielectric constant. If the conformational change is extremely effective, we will have to use a relatively small ε_{eff} (i.e., $\varepsilon' \approx 10$) in equation (6). It is important to point out that this concept has been validated in cases of conformational switches such as the effect of GTP to GDP transition on the Ras/RAF complex [36]. Now with the above view in mind, we examined a wide range of $\varepsilon_{\text{eff.}}$

For low values of ε' we could obtain an interesting tentative gating mechanism that is described schematically in Fig. 10. The figure describes the free energy of the system as a function of the positions of the two protons. We start from state O_R and by transferring the first proton from N to Prd and to P. This a → b path gives a profile similar to the one obtained in Fig. 9 for the corresponding path. We then move the second proton to the Fe-bound OH^- and continue downhill to the chemical trap (P_M). At this point the disappearance of the charge on OH^- destabilizes the proton on Prd but also increases the proton energy on W_3 and W_2. This can lead to a vectorial process, since the barrier for a back transfer of the first proton (from P to N or c → d) is now higher than what was in the first step (b → a). This situation did not occur with larger ε' where the barrier for moving back at state P_M was similar to the barrier of moving forward in state O_R. This mechanism takes advantage of the availability of two paths and of the resulting interaction between the protons on these two paths. It also exploits the trap at the chemical step that prevents the second proton from going backward. We note in this respect that, it is the novel two dimensional diagram presented in Fig. 10, that allows us to examine in a clear logical way these and related proposals. Of course, what has to be established is the validity of a relatively strong charge–charge interaction between the binuclear center and W_3, W_2 and Prd.

Finally, it is interesting to note that we did not explore the possibility that the free energy of penetration on non-protonated water molecules is significantly different in different conformations states (this is, for example, the case in the M → N → O steps in bacteriorhodopsin [38]). Thus, we intend in the future to examine the feasibility that the free energy of forming a water chain is different in different redox states. Although we do not expect this difference to be more than a few kcal/mol, it can help in sustaining a gating mechanism. Of course, obtaining direct structural information about conformational changes (if such changes exist) would be very useful. At any rate, at present our main point is that we have a sufficiently general approach that can be used to calculate key experimental findings, and thus can be used to validate deferent feasible detailed models.

Acknowledgments: We thank Professor Wikstrom for introducing us to this challenging problem and Professor Siegbahn for inspiring discussions. This work was supported financially by NIH Grant R01 GM 40283.

References

[1] Wikström, M.K.F. (1977) Proton pump coupled to cytochrome *c* oxidase in mitochondria. Nature 266, 271–273.
[2] Michel, H., Behr, J., Harrenga, A. and Kannt, A. (1998) Cytochrome *c* oxidase: structure and spectroscopy. Ann. Rev. Biophys. Biomol. Struct. 27, 329–356.
[3] Mills, D.A. and Ferguson-Miller, S. (2002) Influence of structure, pH and membrane potential on proton movement in cytochrome oxidase. Biochim. Biophys. Acta 1555, 96–100.
[4] Ostermeier, C., Harrenga, A., Ermler, U. and Michel, H. (1997) Structure at 2.7 Å resolution of the *Paracoccus denitrificans* two-subunit cytochrome *c* oxidase complexed with an antibody FV fragment. Proc. Natl. Acad. Sci. USA 94, 10547–10553.
[5] Yoshikawa, S., Shinzawa-Itoh, K., Nakashima, R., aono, R., Yamashita, E., Inoue, N., Yao, M., Fei, M.J., Libeu, C.P., Mizushima, T., Yamaguchi, Y., Tomizaki, T. and Tsukihara, T. (1998) Redox-coupled crystal structural changes in bovine heart cytochrome *c* oxidase. Science 280, 1723–1729.
[6] Ferguson-Miller, S. and Babcock, G.T. (1996) Heme/copper terminal oxidases. Chem. Rev. 96, 2889–2907.
[7] Brzezinski, P. and Larsson, G. (2003) Redox-driven proton pumping by heme-copper oxidases. Biochim. Biophys. Acta 1605, 1–13.
[8] Wikstrom, M., Verkhovsky, M.I. and Hummer, G. (2003) atergated mechanism of proton translocation by cytochrome *c* oxidase. Biochim. Biophys. Acta 1604, 61–65.
[9] Olkhova, E., Hutter, M.C., Lill, M.A., Helms, V. and Michel, H. (2004) Dynamic water networks in cytochrome *c* oxidase from *Paracoccus denitrificans* investigated by molecular dynamics simulations. Biophys. J. 86, 1873–1889.
[10] Hofacker, I. and Schulten, K. (1998) Oxygen and proton pathways in cytochrome *c* oxidase. Proteins 30, 100–107.
[11] Siegbahn, P.E.M., lomberg, M.R.A. and Blomberg, M.L. (2003) Theoretical study of the energetics of proton pumping and oxygen reduction in cytochrome oxidase. J. Phys. Chem. B 107, 10946–10955.
[12] Mills, D.A. and Ferguson-Miller, S. (2003) Understanding the mechanism of proton movement linked to oxygen reduction in cytochrome *c* oxidase: lessons from other proteins. FEBS Lett. 545, 47–51.
[13] Namslauer, A. and Brzezinski, P. (2004) Structural elements involved in electron-coupled proton transfer in cytochrome *c* oxidase. FEBS Lett. 567, 103–110.
[14] Warshel, A. (1979) Conversion of light energy to electrostatic energy in the proton pump of Halobacterium halobium. Photochem. Photobiol. 30, 285–290.
[15] Sham, Y., Muegge, I. and Warshel, A. (1999) Simulating proton translocations in proteins: probing proton transfer pathways in the *Rhodobacter sphaeroides* reaction center. Proteins 36, 484–500.
[16] Burykin, A. and Warshel, A. (2003) What really prevents proton transport through*Aquaporin*? Charge self-energy versus proton wire proposals. Biophys. J. 85, 3696–3706.
[17] Warshel, A. and Schlosser, D.W. (1981) Electrostatic control of the efficiency of light-induced electron transfer across membranes. Proc. Natl. Acad. Sci. USA 78, 5564–5568.
[18] Warshel, A. and Parson, W.W. (1991) Computer simulations of electron-transfer reactions in solution and in photosynthetic reaction centers. Ann. Rev. Phys. Chem. 42, 279–309.
[19] Warshel, A. (1991) Computer Simulations of Chemical Reactions in Enzymes and Solution, John Wiley & Sons, New York.
[20] Schutz, C.N. and Warshel, A. (2001) What are the dielectric "constants" of proteins and how to validate electrostatic models. Proteins 44, 400–417.

[21] Braun-Sand, S., Strajbl, M. and Warshel, A. (2004) Studies of proton transocations in biological systems: simulating proton transport in carbonic anhydrase by EVB based models. Biophys. J. 87, 2221–2239.
[22] Warshel, A. and Hwang, J.K. (1986) Simulation of the dynamics of electron-transfer reactions in polar solvents: semiclassical trajectories and dispersed polaron approaches. J. Chem. Phys. 84, 4938–4957.
[23] Olsson, M.H.M., Siegbahn, P.E.M. and Warshel, A. (2004) Simulations of the large kinetic isotope effect and the temperature dependence of the hydrogen atom transfer in *Lipoxygenase*. J. Am. Chem. Soc. 126, 2820–2828.
[24] Warshel, A. and Parson, W.W. (2001) Dynamics of biochemical and biophysical reactions: insight from computer simulations. Quart. Rev. Biophys. 34, 563–670.
[25] Churg, A.K. and Warshel, A. (1986) Control of redox potential of cytochrome *c* and microscopic dielectric effects in proteins. Biochemistry 25, 1675–1681.
[26] Muegge, I., Qi, P.X., Wand, A.J., Chu, Z.T. and Warshel, A. (1997) The reorganization energy of cytochrome *c* revisited. J. Phys. Chem. B 101, 825–836.
[27] Chu, T.Z., Villà, J., Strajbl, M., Schutz, C., Shurki, A. and Warshel, A. (2002) Los Angeles.
[28] Olsson, M.H.M., Hong, G. and Warshel, A. (2003) Frozen density functional free energy simulations of redox proteins: computational studies of the reduction potential of *Plastocyanin* and*Rusticyanin*. J. Am. Chem. Soc. 125, 5025–5039.
[29] Svensson-Ek, M., Abramson, J., Larsson, G., Tornroth, S., Brzezinski, P. and Iwata, S. (2002) The X-ray crystal structures of wild-type and EQ(I-286) mutant cytochrome *c* oxidases from *Rhodobacter sphaeroides*. J. Mol. Biol. 321, 329–339.
[30] Langen, R., Brayer, G.D., Berghuis, A.M., McLendon, G., Sherman, F. and Warshel, A. (1992) Effect of the Asn52–Ile mutation on the redox potential of yeast cytochrome *c*. J. Mol. Biol. 224, 589–600.
[31] Qian, J., et al. (2004) Role of the conserved arginine pair in proton and electron transfer in cytochrome *c* oxidase. Biochemistry 43, 5748–5756.
[32] Kannt, A., Lancaster, R.D. and Michel, H. (1998) The coupling of electron transfer and proton translocation: electrostatic calculations on *Paracoccus dentrificans* cytochrome *c* oxidase. Biophys. J. 74, 708–721.
[33] Åqvist, J. and Luzhkov, V. (2000) Ion permeation mechanism of the potassium channel. Nature 404, 881–884.
[34] Burykin, A., Kato, M. and Warshel, A. (2003) Exploring the origin of the ion selectivity of the KcsA potassium channel. Proteins 52, 412–426.
[35] Warshel, A. and Weiss, R.M. (1981) Energetics of heme–protein interactions in *Hemoglobin*. J. Am. Chem. Soc. 103, 446–451.
[36] Muegge, I., Schweins, T. and Warshel, A. (1998) Electrostatic contributions to protein-protein binding affinities: application to Rap/Raf interaction. Proteins 30, 407–423.
[37] Popovic, D.M. and Stuchebrukhov, A.A. (2004) Electrostatic study of the proton pumping mechanism in bovine heart cytochrome *c* oxidase. J. Am. Chem. Soc. 126, 1858–1871.
[38] Lanyi, J.K. (2004) Bacteriorhodopsin. Annu. Rev. Physiol. 66, 665–688.